



26

Abstract

27 Transport of riverine dissolved carbon (including DOC and DIC) is a crucial process which links
28 terrestrial and aquatic C storages, but is rarely examined in small subtropical mountainous rivers. This
29 study monitored DOC and DIC concentrations on a biweekly basis during regular flow period and at
30 3-hour intervals during two typhoons in 3 small mountainous rivers in southwestern Taiwan between
31 Jan 2014 and Aug 2016. A hydrological model, HBV, and three end-member mixing model were
32 applied to determine the quantities of DOC and DIC transport from different flowpaths. The results
33 showed that the annual DOC and DIC fluxes were 2.7-4.8 and 48.4-54.3 ton-C km⁻² yr⁻¹, which were
34 2- and 20 times higher than the global mean of 1.4 and 2.6 ton-C km⁻² yr⁻¹. The DIC/DOC ratio was
35 14.08, much higher than the mean (1.86) of large rivers worldwide, indicating the high rates of
36 chemical weathering and/or low rates of decomposition in this region. Two typhoons contributed 12-
37 14% of the annual streamflow in only 3 days (~1.0% of the annual time), whereas 15.0-23.5% and 9.2-
38 12.6% of the annual DOC and DIC flux, respectively, suggested that typhoons play a more important
39 role on DOC transport than DIC transport. End-member mixing model suggested that DOC export was
40 mainly from surface runoff, while DIC transport was mainly through deep groundwater. The unique
41 patterns seen in Taiwan SMRs characterized by high dissolved carbon flux, high DIC/DOC ratio, and
42 large transport by intense storms should be taken into consideration when estimating global carbon
43 budgets.

44

45 **Keywords:** dissolved organic carbon, dissolved inorganic carbon, chemical weathering

46

47



48

Introduction

49 Transport of riverine dissolved organic and inorganic carbon (DOC and DIC) transport by river
50 systems is an important linkage among atmospheric, terrestrial and oceanic C storages (Meybeck and
51 Vörösmarty, 1999; Battin et al., 2008). Most DIC is derived from rock weathering, which is largely
52 affected by tectonic activities, responsive to climatic change and closely linked to atmospheric CO₂
53 concentration over geological time scales (Lloret et al., 2011). By contrast, DOC is mainly originated
54 from the decomposition of particulate and dissolved organic matter (POM, DOM). so that is closely
55 associated with different organic sources, bacterial degradation and redox. Both, DOC and DIC
56 availability in freshwater ecosystems control dynamics of primary producers and microbial
57 components in aquatic food webs (Maberly and Madssen, 2002; Maberly, et al., 2015; Giesler et al.,
58 2014). Globally, exoreic rivers can annually export 0.21 and 0.38 Pg-C of DOC and DIC to the ocean
59 (Huang et al., 2012). Although the quantity is small compared with terrestrial C storage (~2300 Pg-
60 C) (Battin et al., 2009; Cole et al., 2007; Ludwig et al., 1998), they have direct effects on
61 downstream ecosystems (Lloret et al., 2013; Atkins et al., 2017). From the compilation of global
62 rivers, large rivers yield approximately 1.4 and 2.6 ton-C km⁻² yr⁻¹ of DOC and DIC, representing
63 21.0% to 37.5% of the global riverine C export. Much of the variation in river export of DOC and
64 DIC depends upon rock lithology, soil properties, climate, runoff, contact time (or flow velocity),
65 aquatic primary production, UVB exposure and streamwater pH (Meybeck and Vörösmarty, 1999;
66 Wymore et al., 2017).

67 With the urgent demand for precise global C budget and modeling, a thorough understanding of
68 riverine C response in different regions is needed (Meybeck and Vörösmarty, 1999). Among the
69 regions, humid tropical/subtropical regions characterized by high productivity and rainfall export
70 large quantities of carbon (Galy et al., 2015; Hilton, 2017), with rivers between 30°N and 30°S
71 transporting ~62% of the global DOC to the ocean (Dai et al., 2012). For these systems, rates of
72 export (2.1 and 3.3 ton-C km⁻² yr⁻¹ of DOC and DIC, respectively) are much greater than the global
73 averages (1.4 and 2.6 for DOC and DIC, respectively) (Huang et al., 2012). Thus, the
74 tropical/subtropical regions are hypothesized as the hotspots of DOC and DIC flux (Degens and
75 Ittekkot, 1985; Lyons et al., 2002). However, studies on DOC and DIC transport in this region are
76 rare.

77 For riverine DOC and DIC transport, the flush hypothesis argued that terrestrial C accumulates
78 in the riparian zone and near-stream hillslopes in regular flow periods and the accumulated C is
79 subsequently flushed by major storms when the water table rises (Mei et al., 2014). Since DOC and
80 DIC have different sources and different transport pathways that are active under different flow



81 regimes, shifts in hydrologic flowpaths will alter the quantity and ratio of DIC: DOC (Walvoord and
82 Striegl, 2007). This has become increasingly important because extreme climate events such as
83 tropical cyclones are projected to become more frequent and intense as a result of global warming
84 (Galy et al., 2015; Heimann and Reichstein, 2008). However, little is known about the processes and
85 their underlying mechanisms of DOC and DIC export to rivers (Atkins et al., 2017). Specifically, the
86 concentration and export of DOC and DIC are hypothesized as being quite different between regular
87 and intense storm periods due to changes in the relative contribution from different flowpaths, but
88 studies up to date provide little information on such shifts of DOC and DIC export.

89 In this study, we monitored DOC and DIC concentration during regular flow periods (biweekly)
90 and during two typhoon events (in a 3-hr interval) at a small subtropical mountainous river in
91 southwestern Taiwan. Based on the analysis of DOC, DIC, and major ions in combination with a
92 hydrological model, HBV, and 3 end-member mixing model, we aimed to identify different flow
93 paths of DOC and DIC transport during regular and high flow periods. The objectives are to 1)
94 compare the riverine DOC and DIC in concentration, flux and ratio of DIC/DOC in three small
95 mountainous rivers in Taiwan; 2) understand the role of typhoon events on annual flux; and 3)
96 identify the shifts in sources of DOC and DIC between regular flow and the typhoon period.

97

98

Material and method

99 Study site

100 The study was conducted at the Tsengwen River in southwestern Taiwan. The Tsengwen River
101 originated from Mt. Dongshui (2,611 m a.s.l.) has a drainage area of 483 km² with a mean terrain
102 slope greater than 50%. The landscape is mainly covered by secondary forests dominated by
103 *Eutrema japonica*, *Areca catechu*, and bamboo with small patches of beetle nut and tea plantations.
104 The annual mean temperature is ~19.8°C with lowest ones in January (17.8°C) and highest in July
105 (21.1°C) (Central Weather Bureau, Taiwan, <http://e-service.cwb.gov.tw/HistoryDataQuery/index.jsp>).
106 The long-term mean annual rainfall is ~3,700 mm yr⁻¹, with approximately 80% occurring from May
107 to October. Tropical cyclones, aka typhoons in Western Pacific, with strong winds and torrential
108 rainfalls, usually lash the area and induce intensive mass movements (e.g. landslides and debris
109 flows) within 2-3 days. These short-term, periodic, extreme events mobilize massive amounts of
110 terrestrial materials to the ocean (Kao et al., 2010; Huang et al., 2017).

111 Three sampling sites were set up: two at tributaries (T1, T2) and one at the mainstream (M3).
112 There is a discharge station at M3 monitored by WRA (Water Resources Agency, Taiwan, [http://](http://www.wra.gov.tw)
113 www.wra.gov.tw) and 14 auto-recording precipitation stations maintained by CWB (Central Weather



114 Bureau, Taiwan). Land-use pattern in the watershed were compiled from aerial photos, satellite
115 imageries, and field surveys during 2004-2006 (National Land Surveying and Mapping Center,
116 2008) (Fig. 1). The proportion of agricultural land (i.e., areca and tea plantation) accounted for 14.0
117 and 23.0% of the area in catchments T1 and T2, but only 7.0% in catchment M3. The legacy of mass
118 movement (i.e., landslide scars) induced by typhoons accounted for 3.0-5.3% of the land area of
119 three catchments.

120

121 **Sampling and chemical analysis**

122 Streamwater was sampled biweekly between January 2014 and August 2016. Additionally, a
123 high frequency (2-3-hr interval) sampling scheme was applied during two typhoon events (Typhoon
124 Matmo, 2014/07/21 to 2014/07/23 and Typhoon Soudelor, 2015/08/06 to 2015/08/08). We took water
125 samples from a bridge by lowering a set of four 1-L HDPE bottles (high-density polyethylene) into
126 the river. An 1-L bottle of water (unfiltered) was used to measure water temperature, pH and
127 electrical conductivity *in situ*. All other water samples were filtered (through pre-weighed and pre-
128 combusted 0.7- μm GF/F filters) and stored at 4°C in a refrigerator for further analyses of major
129 cations and anions. Approximately 50 mL filtrate was acidified by H_3PO_4 for further measurement of
130 DOC (Analytik Jena multi N/C® 3100 Analyzer) with a detection limit of 4 $\mu\text{g/L}$. Major anions (Cl^- ,
131 NO_3^- , SO_4^{2-}) were analyzed by ion chromatography (IC, Methrom® 886 basic plus) with a detection
132 limit of 0.02 mg L^{-1} . Major cations (Na, K, Mg, Ca) were analyzed by ICP-OES (PerkinElmer Inc. -
133 Optima 2100 DV) with a detection limit of 0.02 mg L^{-1} . Using the balance method, the DIC content
134 was calculated from the difference between the total dissolved anions ($\text{TZ}^- = \text{Cl}^- + 2\text{SO}_4^{2-} + \text{HCO}_3^-$
135 $+ \text{NO}_3^-$, in $\mu\text{eq/L}$) and total dissolved cations ($\text{TZ}^+ = \text{Na}^+ + \text{K}^+ + 2\text{Ca}^{2+} + 2\text{Mg}^{2+}$, in $\mu\text{eq/L}$) (Lyons et al.,
136 1992; Zhong et al., 2017).

137

138 **Estimation of DOC and DIC concentration and flux**

139 The concentration and flux of DOC and DIC were estimated by Load Estimator (LOADEST)
140 using the following equation (Runkel et al., 2004):

141

$$142 \quad \ln(F) = a_0 + a_1 \ln(Q) + a_2 \ln(Q^2) + a_3 \sin(2\pi \cdot dtime) + a_4 \cos(2\pi \cdot dtime) \quad \text{Eq. (1)}$$

143

144 where F , Q , and $dtime$ are the flux ($\text{kg km}^{-2} \text{d}^{-1}$), discharge (mm d^{-1}) and Julian day (in decimal
145 form), respectively. In LOADEST, the inputs (Q and Julian day) were decentralized (observation
146 minus average and then over the average) to avoid the co-linearity (Runkel et al., 2004). The



147 coefficient, a_1 and a_2 , are coefficients associated with Q representing the hydrological control. The
 148 other coefficients (a_3 , a_4) which regulate the seasonal variation can mimic the seasonal change in the
 149 concentration and flux. The NSE and Bp are used to examine the differences between observations
 150 and estimations. The NSE (Nash-Sutcliffe efficiency coefficient, Nash and Sutcliffe, 1970) calculates
 151 the explained variances and present the performance between negative infinity to unity. The unity
 152 presents the perfect match between estimations and observations. The Bp shows the yield bias in
 153 percent, defined as the estimations minus the observations over the observations.

154

155 **Streamflow Simulation**

156 A conceptual hydrological model, HBV (Hydrologiska Byråns Vattenbalansavdelning model,
 157 Parajka et al., 2013) was applied to simulate the daily streamflow of the ungauged sites (T1 and T2)
 158 and hourly streamflow of the two typhoon events in M3. The details of the HBV model are described
 159 in detail in Seibert et al. (2012). Briefly, HBV streamflow simulation uses rainfall, temperature,
 160 evapotranspiration (estimated by temperature and humidity) to simulate the streamflow and its
 161 composition. The rainfall, temperature and relative humidity during 2002-2015 from 14 auto-
 162 recording weather stations of CWB were used in our simulations. The daily evapotranspiration was
 163 estimated by Linacre method (Linacre, 1977) through R package of evapotranspiration (Guo et al,
 164 2016). The observed M3 streamflow was then used to adjust the parameters through the performance
 165 measure of NSE. The calibrated parameter set of M3 was applied to T1 and T2 using with their own
 166 climatic inputs to simulate their streamflow. For event simulations, a total of 11 events (during 2005-
 167 2012) in M3 were used to calibrate the event-based parameter set. We also affirmed the reliability of
 168 the streamflow composition derived from the HBV models using the electrical conductivity (EC) and
 169 ions [Mg^{2+} , Ca^{2+} , and Cl^-] through a 3-endmember mixing model.

170

171 **End-member mixing analysis**

172 Conceptually, the streamflow is composed of the rapid surface runoff (RSR), subsurface runoff
 173 (SSR), and deep groundwater (DG) during rainstorms. DOC and DIC concentrations of the samples
 174 collected during each typhoon event were the mixture from the three runoffs and the 3-end-member
 175 mixing model is used to estimate the relative contributions of the three runoffs. With the assumption
 176 of time-invariant sources and mass balance, the sources of DOC and DIC transported by the three
 177 runoff paths can be estimated using the following three equations:

$$178 \quad 1 = [Q]_{RSR,i} + [Q]_{SSR,i} + [Q]_{DG,i} \quad \text{Eq. (2)}$$

$$179 \quad [C]_{River,i} = [C]_{RSR}[Q]_{RSR,i} + [C]_{SSR}[Q]_{SSR,i} + [C]_{DG}[Q]_{DG,i} \quad \text{Eq. (3)}$$



180 Here, $[Q]$ is the proportion of the three runoffs, with the sum of the three should equal to 1 at any
181 time step. The observed elemental concentration, $[C]_{\text{River},i}$ in the stream is regarded as the mixing
182 result among $[C]_{\text{RSR}}$, $[C]_{\text{SSR}}$, and $[C]_{\text{DG}}$. Here, the unknown end members can be estimated by the
183 observed and the simulated $[C]_{\text{River},i}$. The performance of simulated concentration was also evaluated
184 by the NSE.
185



186

187

188

Results

189 Temporal dynamics of DOC and DIC concentration and flux

190 Most of the observed DOC concentrations of the three sites were less than 200 μM (or 2.4 mg-
191 C L^{-1}) with no prominent seasonality, but rapid increases during the two typhoon events (Fig. 2). In
192 contrast, DIC concentrations varied widely from 1500 to 3500 μM and were higher in the dry season
193 (November to the next April) and substantially dropped during typhoons. The LOADEST
194 satisfactorily estimated daily flux of DOC and DIC, with R^2 greater than 0.96, NSE of 0.88-0.98 and
195 Bp of 0.4%-6.1% (Table 1). The good performance in calculation of daily flux supports the validity
196 of estimated annual DOC and DIC fluxes from the load estimation model (LOADEST). On the other
197 hand, LOADEST calculated daily concentrations of DOC and DIC moderately well, with R^2 of 0.34-
198 0.55, and NSE of 0.31-0.55 for DOC, slightly better than the R^2 of 0.51-0.63 and NSE of 0.50-0.59
199 for DIC.

200 The simulated mean DOC concentration of the three sites varied from 48 μM in the dry season
201 to 147 μM in the wet season (May to October), with the annual mean of 137 μM , and the simulated
202 mean DIC concentration of the three sites varied from 2216 μM in the dry season to 1928 μM in the
203 wet season, with the annual mean of 1951 μM (Table 2). The monthly DOC and DIC fluxes
204 represented a distinct seasonal variation (Fig. 3). In general, the estimated DOC flux was 3.7 ton-C
205 $\text{km}^{-2} \text{yr}^{-1}$, with ~95% contributed during the wet season and ~5% during the dry season, mostly due
206 to higher discharge in the wet season. The annual DIC flux was approximately 52.1 ton-C $\text{km}^{-2} \text{yr}^{-1}$,
207 with ~88% from the wet season and ~12% from the dry season. A notable low export of DOC and
208 DIC in June and July 2015 during wet season was attributed by that the rainfall was only 62 and 300
209 mm month^{-1} . Specifically, the variations of DOC and DIC concentrations of T1 and M3 during
210 Matmo and Soudelor were shown (Fig. 4). The dataset of DOC and DIC at site T2 was incomplete
211 and not shown due to a road damage during Soudelor. The DOC concentrations were ~100 μM in
212 low flow periods and it increased rapidly to more than 350 and ~270 μM for T1 and M3 during
213 typhoon, respectively, just before the discharge peaks. After the discharge peaks, the DOC
214 concentration quickly decreased to ~100 μM returned to levels prior to the typhoons. The DIC
215 concentration showed an opposite temporal pattern compared to DOC. The DIC concentration was
216 ~2500 μM in low flow periods, however, as rainstorm begins it gradually decreased with the increase
217 of discharge to only 900 and 1200 μM in T1 and M2, respectively. During the recession period, the
218 DIC concentration gradually increased to 2000 and 1500 μM for T1 and M3, respectively. The



219 recovery of DIC concentration to pre-typhoon levels was much slower than that of DOC
220 concentration. The monthly and event DOC and DIC transport indicated that discharge is the key to
221 the seasonal differences in dissolved carbon flux.

222

223 **Streamflow composition and sources of DIC and DOC**

224 After the calibration with 11 historical events (since 2005-2012), the streamflow simulations of
225 Matmo and Soudelor by HBV agreed well with the observed discharge as indicated by the high NSE
226 values (0.89 and 0.79, respectively). In this modeling approach, rapid surface runoff (RSR)
227 contributed approximately 40-50% to the total flow, subsurface runoff (SSR) accounted for
228 approximately 25%, and the rest was attributed to deep groundwater (DG). The 3-endmember
229 mixing model accompanying with Ca^{2+} , Mg^{2+} , and EC used to evaluate the fractions of different
230 runoffs which performed moderately well, with NSE values of 0.76, 0.73 and 0.68 for Ca^{2+} , Mg^{2+} ,
231 and EC, respectively.

232 Through the simple streamflow simulation and validation of its composition, the proportions of
233 runoff, DOC and DIC fluxes from the different runoffs were identified (Table 3) and the temporal
234 variation of DOC and DIC fluxes transported by the three runoffs were shown in Fig. 5. The two
235 typhoons accounted for 12% and 14.0% of the annual discharge, which consisted only 1.0% of the
236 two year sampling time (i.e., six days). DOC exported during Typhoon Matmo and Soudelor, were
237 $382.5 \text{ kg-C km}^{-2}$ (or 15.0%) and 744 kg-C km^{-2} (23.5%), respectively, of the annual yield. Among the
238 three runoffs, RSR was the main contributor delivering ~40-48% of DOC export during the typhoon
239 periods, followed by SSR, ~37%, while the DG only contributed ~20%. For DIC, the two events
240 exported $3999.4 \text{ kg-C km}^{-2}$ (9.2%) and $6790.3 \text{ kg-C km}^{-2}$ (12.6%) of the annual flux, respectively.
241 The RSR, SSR, and DG transported ~29%, 21%, and 50% of DIC during the two typhoon events.
242 Since DG accounted for a low proportion of discharge, the high DIC flux from groundwater was
243 likely attributed to the extreme high DIC concentration. In sum, the RSR is a predominant factor for
244 transporting DOC due to the large amount, whereas the DG plays a key role in DIC export owing to
245 the extreme high DIC concentration in groundwater storage.



246

247

Discussion

248 **Dissolved carbon Dynamics in Taiwan SMR**

249 Global mean DOC and DIC concentrations of large rivers were 479 and 858 μM , respectively,
250 which were considerably greater than the means of 199 and 408 μM , respectively, for many SMRs
251 around the world (Table 4) (Meybeck and Vörösmarty, 1999). However, the global mean annual
252 fluxes of DOC and DIC of large rivers were 1.4 and 2.6 $\text{ton-C km}^{-2} \text{yr}^{-1}$, respectively, much lower
253 than means of 2.5 and 7.01 $\text{ton-C km}^{-2} \text{yr}^{-1}$ for SMRs. In Oceania, which is characterized by high
254 temperature, and abundant rainfall, the mean DOC and DIC concentrations were 399 and 1,781 μM
255 (Huang et al., 2012). While the DOC concentration, ranges between the means of global large rivers
256 and SMRs, the DIC concentration was much higher than the global means of both large rivers and
257 SMRs (Table 4). Due to high rainfall, the fluxes of DOC and DIC in Oceania were 8.0 and 34.0 ton-
258 $\text{C km}^{-2} \text{yr}^{-1}$, much higher than the global means of large rivers and SMRs. The lower concentration,
259 but higher flux in the SMRs and Oceania islands suggests greater importance of discharge on DOC
260 and DIC export.

261 Globally, DOC is positively correlated with discharge, soil organic carbon (SOC) content, and
262 negatively correlated with slope steepness (Ludwig et al., 1996a; Ludwig et al., 1996b). Another
263 study of global DOC flux indicated that the soil C: N ratio could be a dominant predictor for riverine
264 DOC flux (Aitkenhead and McDowell, 2000). In Taiwan, the abundant discharge has been well
265 recognized. For SOC and slope, Schomakers et al. (2017) reported that six years after a landslide, the
266 SOC in shallow soils ($< 100 \text{ cm}$) was only $2.9 \pm 0.6 \text{ ton-C ha}^{-1}$ and it increased to only $75.7 \pm 5.0 \text{ ton-C}$
267 ha^{-1} after 41 years, being still lower than those of the reference sites ($75\text{-}150 \text{ ton-C ha}^{-1}$). The steep
268 slopes, which result in restricted contact time between discharge water and the soils (Ludwig et al.,
269 1996; Hale and McDonnell, 2016), may partly explain the low riverine DOC concentration in SMRs
270 and Oceania islands. For aquatic ecosystems, the steep landscape morphology, which is characterized
271 by fast flows and short water residence times in the stream, limits an intense cycling of dissolved
272 organic matter (DOM) in lotic ecosystems (Stutter et al., 2013). The low SOC and high flow
273 velocities likely result in the low, but incessant DOC supply and lead to low productivity of lotic
274 ecosystems. However, due to abundant precipitation, DOC fluxes are still high.

275 Riverine DIC originated from rock weathering generally increases with increasing temperature,
276 runoff and physical erosion rate (Maher and Chamberlain, 2014). Thus, the DIC concentration in
277 SMRs gradually decreases with the latitude gradient (Table 4). However, the DIC concentrations are
278 greater than 1,000 μM in Oceania islands, which is two times higher than the global average, most



279 likely due to the large physical erosion and very high chemical weathering rates associated to the
280 steep topography, high precipitation and high temperature (West, 2012). In our study, the DIC
281 concentration and flux are as high as $\sim 1951 \mu\text{M}$ and $52.1 \text{ ton-C km}^{-2} \text{ yr}^{-1}$. The DIC concentration was
282 as high as the concentration in the karst landscape (characterized by extraordinary high DIC
283 concentrations), Wujiang (Zhong et al., 2017). The high concentrations in combination with
284 abundant rainfall and high temperature elevate our DIC flux up to 10-fold higher than the global
285 mean of $2.6 \text{ ton-C km}^{-2} \text{ yr}^{-1}$ (Meybeck and Vörösmarty, 1999; Dessert et al., 2003). In addition, high
286 physical erosion rates which would expose fresh rocks enhancing interaction with water also provide
287 conditions favorable for chemical weathering (Larsen et al., 2012; Larsen et al., 2014; Lyons et al.,
288 2005). The unique environmental setting resulted in the extremely high DIC concentration and flux.

289 The DIC/DOC ratios of the global large rivers, SMRs, and Oceania were 1.86, 2.80, and 4.25,
290 respectively (Table 4). The DIC/DOC ratio could be used for improving the understanding of
291 biogeochemical C processes such as photosynthesis and organic carbon mineralization in streams.
292 DIC is the essential source for autotrophic photosynthesis and DOC for microbial decomposition
293 (Lloret et al., 2011; Atkins et al., 2017). The global mean DIC/DOC ratio is ~ 1.86 , indicating that
294 DOC accounts for 35% of the total dissolved carbon in global large rivers. The DIC/DOC ratio in
295 SMRs around the world is ~ 2.8 , which could be due to: 1. large DIC supply; 2. limited DIC
296 consumption, and 3. limited DOM decomposition. The DIC/DOC ratios in our catchments were
297 14.08, much higher than those in other rivers of Oceania (4.25) and rarely seen at these ranges across
298 the globe. From the viewpoint of a carbon mass balance, the export of dissolved carbon from SMRs
299 and Oceania islands is contributed mainly from DIC, which is different from that of the global large
300 rivers. Therefore, when discussing global carbon dynamics, The SMRs and Oceania islands which
301 account for the subtle area, might have a disproportional dissolved carbon flux, particularly during
302 typhoon events. It also implied that the dissolved carbon export in SMRs and Oceania islands is
303 sensitive to environmental change (e.g. rainfall intensification and global warming). .

304

305 **Sources of dissolved carbon combination in Different Flow Regimes**

306 The estimated DOC and DIC transport from different runoffs and the observed concentration-
307 discharge (C-Q) relationships for DOC and DIC were illustrated in Fig. 6. In the C-Q relationship
308 (the plots in the center of the figure), the streamflow enhances the DOC concentration, but dilutes the
309 DIC concentration (e.g. Jin et al., 2014; Battin et al., 2003; Wymore et al., 2017; Zhong et al., 2017).
310 The tighter C-Q relationship for DIC than DOC indicates that the mechanism of DOC transport
311 cannot solely be explained by discharge control, possibly because microbial decomposition also



312 played an important role (Yeh et al., submitted). Based on the source identification using the 3 end-
313 member mixing model (Eq. 2 and 3), the DOC concentrations of the three sources (RSR, rapid
314 surface runoff; SSR, subsurface runoff; and DG, deep groundwater) were estimated to be 108, 206,
315 and 86 μM , respectively. The estimated DOC concentrations were one to two orders of magnitude
316 lower than the total DOC in the topsoils (0-10 cm) measured using ultrasonic-induced soil aggregate
317 breakdown method (3.6-11.3 mM, Schomakers et al., unpublished data). The much lower estimated
318 DOC concentrations possibly could be due to that the ultrasonic-induced soil aggregate breakdown
319 method expels all DOC from the soil, while our estimate only includes DOC transported by RSR.
320 Due to the short contact time of water with land surface during extreme events, the DOC might not
321 be disaggregated and transported out to streamwater. The lower DOC concentration in DG partly
322 explains the low riverine DOC concentration in the low flow period, since DG is the main
323 contributor of baseflow. During high flows, abundant RSR and SSR rapidly surge and flush
324 terrestrial allochthonous DOC from soils into the stream leading to the enhancement mode in the C-
325 Q relationship, which is consistent with the flush hypothesis (Mei et al., 2014). On the other hand,
326 the DIC concentration increased from 915 to 2,297 μM with increasing soil depth, following the
327 weathering gradient. The much higher DIC concentration in DG indicated that weathering likely took
328 place in the deep rocks (Calmels et al., 2011). Thus, the riverine DIC concentration would be
329 strongly diluted by a large contribution of RSR and SSR during high flows.

330 Furthermore, two interesting questions could be addressed. First, what is the main DOC source in
331 stream water during typhoon periods? Some studies suggested that the riparian zone is the main
332 source of DOC during a rainstorm, as described by the flush hypothesis (Winterdahl et al., 2011;
333 Wymore et al., 2017). However, hillslopes, as illustrated in our conceptual model, have also been
334 proven an important source of DOC when rainstorms connect the hillslopes to stream by runoffs (i.e.,
335 hydrological connectivity, Birkel et al., 2014). Future research using isotope techniques may help to
336 clarify the relative importance of riparian zones and hillslopes on DOC export. Another interesting
337 question is the changes in the relative contributions from the three sources between regular periods
338 and extreme storm events in SMRs. Not only the change of DOC concentration, but also DOC
339 composition. High water level washed out the lower molecular weight of DOC from the subsurface
340 layer (Lloret et al., 2011). The physical force associated with heavy storms such as typhoons can
341 transport a tremendous amount of terrestrial material to streams. In our study, one typhoon could
342 transport 12-14% of annual streamflow, with 15-23.5% and 9.2-12.6% of annual DOC and DIC
343 fluxes. On average, there are 3-6 typhoons making landfall to Taiwan (Lin et al., 2017). Thus, the
344 annual DOC and DIC flux contributed by typhoon storms may be as high as ~50% and 30%,
345 respectively. Lloret et al. (2013) reported that flash floods account for 60% of the annual DOC export



346 and 25-45% of the DIC export in small tropical volcanic islands, highlighting the important role of
347 these extreme meteorological events. With the projected global warming, the frequency and intensity
348 of extreme rainfall is expected to increase, while mild rainfall tends to be reduced in Taiwan (Liu et
349 al., 2009). Thus, streamflow may become scater in the dry season and higher and more variable in
350 the wet season (Huang et al., 2014; Lee et al., 2015). Under such conditions, the difference in
351 DIC/DOC ratio between dry and wet season would be exaggerated, with the potential of altering the
352 biogeochemical C processes in aquatic ecosystems.

353

354



355

Conclusions

356 In this study, we found that although the mean DOC concentrations in SMRs in southwestern Taiwan
357 was as low as 99-174 μM , much lower than the global mean of 479 μM , the DOC flux was very
358 high, 2.7-4.8 $\text{ton-C km}^{-2} \text{ yr}^{-1}$, 2-3 times the global average of 1.4 $\text{ton-C km}^{-2} \text{ yr}^{-1}$. The low DOC
359 concentrations is likely attributed to steep landscape morphology which limits the contact time of
360 water with soils. On the other hand, the abundant rainfall still led to the high DOC flux in the SMRs
361 revealing the importance of hydrological control on DOC export and the supply is incessant. By
362 contrast, DIC concentration and flux are as high as 1805-2099 μM and 48.4-54.3 $\text{ton-C km}^{-2} \text{ yr}^{-1}$,
363 much higher than the global mean of 858 μM and 2.6 $\text{ton-C km}^{-2} \text{ yr}^{-1}$. The extreme high DIC
364 concentration and flux resulted from active chemical weathering, representing a high supply for
365 aquatic photosynthesis. From the perspective of global large rivers, the mean DIC/DOC ratio of 1.86
366 indicated that the DOC accounts for 35% of the total dissolved carbon export. However, our much
367 higher DIC/DOC ratio (14.08) indicates that DOC only accounts for ~6.6% of the dissolved carbon,
368 which might not be only unusual in Taiwan, but for other SMRs.

369 The DOC and DIC fluxes during two typhoon events (accounted for ~1.0% of the annual time)
370 contributed 15-23% and 9.2-12.6% of annual DOC and DIC flux, respectively, highlighting the role
371 of extreme events DOC and DIC transport. The enhancement of DOC during higher streamflow
372 indicates the hillslope or riparian zone could be an important DOC source which was
373 disproportionally flushed out during high flow regime. In contrast, the dilution effect of DIC
374 associated with high streamflow implies that there was a large amount of runoff passed through
375 sources with low DIC (e.g., land surface). The modeling work demonstrated the patterns of DOC and
376 DOC transport were rapidly transferred during high and low flow regimes. The DOC was mainly
377 from the soil surface that was flushed out by surface runoff, whereas the DIC is mainly transported
378 by deep groundwater. However, the linkage of different C storages to streams requires further
379 investigations. Riparian zones and hillslopes, both have been suggested as the major DOC source
380 during rainstorms, but the exact sources and their relative importance during different flow regimes
381 in SMRs have not been comprehensively addressed. The high dissolved carbon flux, high DIC/DOC
382 ratio, and large transport by rainstorms in SMRs should be considered in estimating global carbon
383 budgets.

384



385

386

Acknowledgement

387 This study was sponsored by Taiwan Ministry of Science and Technology, (MOST 105-2116-M-002-

388 022, MOST 102-2923-M-002-001-MY3), Austrian Science Fund (FWF I 1396-B16) and National

389 Taiwan University (105R3208). We sincerely appreciate Prof. Teng-Chiu Lin for proofreading this

390 manuscript and the reviewers for their constructive comments.

391



392

393

Reference

- 394 Aitkenhead, J. A., and McDowell, W. H.: Soil C:N ratio as a predictor of annual riverine DOC flux at
395 local and global scales, *Global Biogeochem. Cy.*, 14, 127-138, [10.1029/1999GB900083](https://doi.org/10.1029/1999GB900083), 2000.
- 396 Alin, S. R., Aalto, R., Goni, M. A., Richey, J. E., and Dietrich, W. E.: Biogeochemical
397 characterization of carbon sources in the Strickland and Fly rivers, Papua New Guinea, *Journal*
398 *of Geophysical Research*, 113, [10.1029/2006jf000625](https://doi.org/10.1029/2006jf000625), 2008.
- 399 Argerich, A., Haggerty, R., Johnson, S. L., Wondzell, S. M., Dosch, N., Corson-Rikert, H., Ashkenas,
400 L. R., Pennington, R., and Thomas, C. K.: Comprehensive multiyear carbon budget of a
401 temperate headwater stream, *J Geophys Res-Bioge*, 121, 1306-1315, [10.1002/2015jg003050](https://doi.org/10.1002/2015jg003050),
402 2016.
- 403 Atkins, M. L., Santos, I. R., and Maher, D. T.: Seasonal exports and drivers of dissolved inorganic
404 and organic carbon, carbon dioxide, methane and delta13C signatures in a subtropical river
405 network, *Sci. Total Environ.*, 575, 545-563, [10.1016/j.scitotenv.2016.09.020](https://doi.org/10.1016/j.scitotenv.2016.09.020), 2017.
- 406 Battin, T. J., Kaplan, L. A., Newbold, J. D., and Hendricks, S. P.: A mixing model analysis of stream
407 solute dynamics and the contribution of a hyporheic zone to ecosystem function, *Freshwater*
408 *Biol.*, 48, 995-1014, [10.1046/j.1365-2427.2003.01062.x](https://doi.org/10.1046/j.1365-2427.2003.01062.x), 2003.
- 409 Battin, T. J., Kaplan, L. A., Findlay, S., Hopkinson, C. S., Marti, E., Packman, A. I., Newbold, J. D.,
410 and Sabater, F.: Biophysical controls on organic carbon fluxes in fluvial networks, *Nat Geosci*,
411 1, 95-100, [10.1038/ngeo101](https://doi.org/10.1038/ngeo101), 2008.
- 412 Battin, T. J., Luysaert, S., Kaplan, L. A., Aufdenkampe, A. K., Richter, A., and Tranvik, L. J.: The
413 boundless carbon cycle, *Nat Geosci*, 2, 598-600, [10.1038/ngeo618](https://doi.org/10.1038/ngeo618), 2009.
- 414 Birkel, C., Soulsby, C., and Tetzlaff, D.: Integrating parsimonious models of hydrological
415 connectivity and soil biogeochemistry to simulate stream DOC dynamics, *Journal of*
416 *Geophysical Research: Biogeosciences*, 119, 1030-1047, [10.1002/2013JG002551](https://doi.org/10.1002/2013JG002551), 2014.
- 417 Calmels, D., Galy, A., Hovius, N., Bickle, M., West, A. J., Chen, M. C., and Chapman, H.:
418 Contribution of deep groundwater to the weathering budget in a rapidly eroding mountain belt,
419 Taiwan, *Earth and Planetary Science Letters*, 303, 48-58, [10.1016/j.epsl.2010.12.032](https://doi.org/10.1016/j.epsl.2010.12.032), 2011.
- 420 Calmels, D., Gaillardet, J., and Francois, L.: Sensitivity of carbonate weathering to soil CO₂
421 production by biological activity along a temperate climate transect, *Chemical Geology*, 390,
422 74-86, [10.1016/j.chemgeo.2014.10.010](https://doi.org/10.1016/j.chemgeo.2014.10.010), 2014.
- 423 Cole, J. J., Prairie, Y. T., Caraco, N. F., McDowell, W. H., Tranvik, L. J., Striegl, R. G., Duarte, C.
424 M., Kortelainen, P., Downing, J. A., Middelburg, J. J., and Melack, J.: Plumbing the global
425 carbon cycle: Integrating inland waters into the terrestrial carbon budget, *Ecosystems*, 10, 171-
426 184, 2007.
- 427 Dai, M., Yin, Z., Meng, F., Liu, Q., and Cai, W.-J.: Spatial distribution of riverine DOC inputs to the
428 ocean: an updated global synthesis, *Current Opinion in Environmental Sustainability*, 4, 170-
429 178, [10.1016/j.cosust.2012.03.003](https://doi.org/10.1016/j.cosust.2012.03.003), 2012.
- 430 Degens, E. T., and Ittekkot, V.: Particulate organic carbon an overview, *Transport of carbon and*
431 *minerals in major world rivers, lakes and estuaries. Mitt. Geol.-Palaont. Inst. Univ. Hamburg*, 7-
432 27, 1985.
- 433 Dessert, C., Dupré, B., Gaillardet, J., François, L. M., and Allègre, C. J.: Basalt weathering laws and
434 the impact of basalt weathering on the global carbon cycle, *Chemical Geology*, 202, 257-273,
435 <https://doi.org/10.1016/j.chemgeo.2002.10.001>, 2003.
- 436 Freeman, C., Fenner, N., Ostle, N. J., Kang, H., Dowrick, D. J., Reynolds, B., Lock, M. A., Sleep, D.,
437 Hughes, S., and Hudson, J.: Export of dissolved organic carbon from peatlands under elevated
438 carbon dioxide levels, *Nature*, 430, 195-198, 2004.
- 439 Galy, V., Peucker-Ehrenbrink, B., and Eglinton, T.: Global carbon export from the terrestrial
440 biosphere controlled by erosion, *Nature*, 521, 204-207, [10.1038/nature14400](https://doi.org/10.1038/nature14400), 2015.



- 441 Giesler, R., Lyon, S. W., Mörth, C. M., Karlsson, J., Karlsson, E. M., Jantze, E. J., Destouni, G., and
442 Humborg, C.: Catchment-scale dissolved carbon concentrations and export estimates across six
443 subarctic streams in northern Sweden, *Biogeosciences*, 11, 525-537, 10.5194/bg-11-525-2014,
444 2014.
- 445 Guo, D. L., Westra, S., and Maier, H. R.: An R package for modelling actual, potential and reference
446 evapotranspiration, *Environmental Modelling & Software*, 78, 216-224,
447 10.1016/j.envsoft.2015.12.019, 2016.
- 448 Hale, V. C., and McDonnell, J. J.: Effect of bedrock permeability on stream base flow mean transit
449 time scaling relations: 1. A multiscale catchment intercomparison, *Water Resour. Res.*, 52,
450 1358-1374, 10.1002/2014wr016124, 2016.
- 451 Heimann, M., and Reichstein, M.: Terrestrial ecosystem carbon dynamics and climate feedbacks,
452 *Nature*, 451, 289-292, 10.1038/nature06591, 2008.
- 453 Hilton, R. G.: Climate regulates the erosional carbon export from the terrestrial biosphere,
454 *Geomorphology*, 277, 118-132, <https://doi.org/10.1016/j.geomorph.2016.03.028>, 2017.
- 455 Huang, T.-H., Fu, Y.-H., Pan, P.-Y., and Chen, C.-T. A.: Fluvial carbon fluxes in tropical rivers,
456 *Current Opinion in Environmental Sustainability*, 4, 162-169, 10.1016/j.cosust.2012.02.004,
457 2012.
- 458 Huang, H., Chen, D. J., Zhang, B. F., Zeng, L. Z., and Dahlgren, R. A.: Modeling and forecasting
459 riverine dissolved inorganic nitrogen export using anthropogenic nitrogen inputs, hydroclimate,
460 and land-use change, *J. Hydrol.*, 517, 95-104, 10.1016/j.jhydrol.2014.05.024, 2014.
- 461 Huang, J.-C., Milliman, J. D., Lee, T.-Y., Chen, Y.-C., Lee, J.-F., Liu, C.-C., Lin, J.-C., and Kao, S.-
462 J.: Terrain attributes of earthquake- and rainstorm-induced landslides in orogenic mountain Belt,
463 *Taiwan, Earth Surface Processes and Landforms*, 10.1002/esp.4112, 2017.
- 464 Jarvie, H. P., King, S. M., and Neal, C.: Inorganic carbon dominates total dissolved carbon
465 concentrations and fluxes in British rivers: Application of the THINCARB model -
466 Thermodynamic modelling of inorganic carbon in freshwaters, *Science of the Total
467 Environment*, 575, 496-512, 10.1016/j.scitotenv.2016.08.201, 2017.
- 468 Jin, J., Zimmerman, A. R., Moore, P. J., and Martin, J. B.: Organic and inorganic carbon dynamics in
469 a karst aquifer: Santa Fe River Sink-Rise system, north Florida, USA, *Journal of Geophysical
470 Research: Biogeosciences*, 119, 340-357, 10.1002/2013JG002350, 2014.
- 471 Kao, S. J., Dai, M., Selvaraj, K., Zhai, W., Cai, P., Chen, S. N., Yang, J. Y. T., Liu, J. T., Liu, C. C.,
472 and Syvitski, J. P. M.: Cyclone-driven deep sea injection of freshwater and heat by hyperpycnal
473 flow in the subtropics, *Geophys Res Lett*, 37, L21702, 10.1029/2010GL044893, 2010.
- 474 Larsen, I. J., and Montgomery, D. R.: Landslide erosion coupled to tectonics and river incision,
475 *Nature Geosci*, 5, 468-473,
476 <http://www.nature.com/ngeo/journal/v5/n7/abs/ngeo1479.html#supplementary-information>,
477 2012.
- 478 Larsen, I. J., Almond, P. C., Eger, A., Stone, J. O., Montgomery, D. R., and Malcolm, B.: Rapid Soil
479 Production and Weathering in the Western Alps, New Zealand, *Science*,
480 10.1126/science.1244908, 2014.
- 481 Lee, T.-Y., Hong, N.-M., Shih, Y.-T., Huang, J.-C., and Kao, S.-J.: The sources of streamwater to
482 small mountainous rivers in Taiwan during typhoon and non-typhoon seasons, *Environ Sci
483 Pollut Res*, 1-18, 10.1007/s11356-015-5183-2, 2015.
- 484 Li, Y.-H.: Denudation of Taiwan Island since the Pliocene Epoch, *Geology*, 4, 105-107,
485 10.1130/0091-7613(1976)4<105:DOTIST>2.0.CO;2, 1976.
- 486 Lin, K. C., Hamburg, S. P., Wang, L. X., Duh, C. T., Huang, C. M., Chang, C. T., and Lin, T. C.:
487 Impacts of increasing typhoons on the structure and function of a subtropical forest: reflections
488 of a changing climate, *Scientific Reports*, 7, ARTN 4911, 10.1038/s41598-017-05288-y, 2017.
- 489 Linacre, E. T.: A simple formula for estimating evaporation rates in various climates, using
490 temperature data alone, *Agricultural meteorology*, 18, 409-424, 1977.



- 491 Liu, S. C., Fu, C. B., Shiu, C. J., Chen, J. P., and Wu, F. T.: Temperature dependence of global
492 precipitation extremes, *Geophys Res Lett*, 36, L17702, 10.1029/2009gl040218, 2009.
- 493 Lloret, E., Dessert, C., Gaillardet, J., Albéric, P., Crispi, O., Chaduteau, C., and Benedetti, M. F.:
494 Comparison of dissolved inorganic and organic carbon yields and fluxes in the watersheds of
495 tropical volcanic islands, examples from Guadeloupe (French West Indies), *Chemical Geology*,
496 280, 65-78, 10.1016/j.chemgeo.2010.10.016, 2011.
- 497 Lloret, E., Dessert, C., Pastor, L., Lajeunesse, E., Crispi, O., Gaillardet, J., and Benedetti, M. F.:
498 Dynamic of particulate and dissolved organic carbon in small volcanic mountainous tropical
499 watersheds, *Chemical Geology*, 351, 229-244, 10.1016/j.chemgeo.2013.05.023, 2013.
- 500 Ludwig, W., Suchet, P., Munhoven, G., and Probst, J.-L.: Atmospheric CO₂ consumption by
501 continental erosion: Present-day controls and implications for the last glacial maximum, *Glob.*
502 *Planet. Change*, 16, 107-120, 10.1016/S0921-8181(98)00016-2, 1998.
- 503 Ludwig, W., AmiotteSuchet, P., and Probst, J. L.: River discharges of carbon to the world's oceans:
504 Determining local inputs of alkalinity and of dissolved and particulate organic carbon, *Cr Acad*
505 *Sci Li A*, 323, 1007-1014, 1996a.
- 506 Ludwig, W., Probst, J.-L., and Kempe, S.: Predicting the oceanic input of organic carbon by
507 continental erosion, *Global Biogeochem. Cy.*, 10, 23-41, 10.1029/95gb02925, 1996b.
- 508 Lyons, T. W., and Berner, R. A.: Carbon-sulfur-iron systematics of the uppermost deep-water
509 sediments of the Black Sea, *Chemical Geology*, 99, 1-27, [https://doi.org/10.1016/0009-](https://doi.org/10.1016/0009-2541(92)90028-4)
510 [2541\(92\)90028-4](https://doi.org/10.1016/0009-2541(92)90028-4), 1992.
- 511 Lyons, W. B., Nezat, C. A., Carey, A. E., and Hicks, D. M.: Organic carbon fluxes to the ocean from
512 high-standing islands, *Geology*, 30, 443-446, [Doi 10.1130/0091-](https://doi.org/10.1130/0091-7613(2002)030<0443:Ocfito>2.0.Co;2)
513 [7613\(2002\)030<0443:Ocfito>2.0.Co;2](https://doi.org/10.1130/0091-7613(2002)030<0443:Ocfito>2.0.Co;2), 2002.
- 514 Lyons, W. B., Carey, A. E., Hicks, D. M., and Nezat, C. A.: Chemical weathering in high-sediment-
515 yielding watersheds, New Zealand, *Journal of Geophysical Research: Earth Surface*, 110,
516 F01008, 10.1029/2003JF000088, 2005.
- 517 Maberly, S. C., and Madsen, T. V.: Freshwater angiosperm carbon concentrating mechanisms:
518 processes and patterns, *Funct. Plant Biol.*, 29, 393-405, 2002.
- 519 Maberly, S. C., Berthelot, S. A., Stott, A. W., and Gontero, B.: Adaptation by macrophytes to
520 inorganic carbon down a river with naturally variable concentrations of CO₂, *J. Plant Physiol.*,
521 172, 120-127, 10.1016/j.jplph.2014.07.025, 2015.
- 522 Maher, K., and Chamberlain, C. P.: Hydrologic Regulation of Chemical Weathering and the Geologic
523 Carbon Cycle, *Science*, 343, 1502-1504, 2014.
- 524 Mei, Y., Hornberger, G. M., Kaplan, L. A., Newbold, J. D., and Aufdenkampe, A. K.: The delivery of
525 dissolved organic carbon from a forested hillslope to a headwater stream in southeastern
526 Pennsylvania, USA, *Water Resour. Res.*, 50, 5774-5796, 10.1002/2014WR015635, 2014.
- 527 Meybeck, M., and Vörösmarty, C.: Global transfer of carbon by rivers, *Global Change Newsletter*,
528 37, 18-19, 1999.
- 529 Parajka, J., Viglione, A., Rogger, M., Salinas, J. L., Sivapalan, M., and Blöschl, G.: Comparative
530 assessment of predictions in ungauged basins - Part 1: Runoff-hydrograph studies, *Hydrol.*
531 *Earth Syst. Sci.*, 17, 1783-1795, 10.5194/hess-17-1783-2013, 2013.
- 532 Runkel, R. L., Crawford, C. G., and Cohn, T. A.: Load estimator (LOADEST): a FORTRAN
533 program for estimating constituent loads in streams and rivers, Report 4-A5, 2004.
- 534 Schomakers, J., Jien, S.-H., Lee, T.-Y., Huang, J.-C., Hseu, Z.-Y., Lin, Z. L., Lee, L.-C., Hein, T.,
535 Mentler, A., and Zehetner, F.: Soil and biomass carbon re-accumulation after landslide
536 disturbances, *Geomorphology*, 288, 164-174, <http://doi.org/10.1016/j.geomorph.2017.03.032>,
537 2017.
- 538 Schomakers, J., Mayer, H., Lee, J.Y., Lee, T.Y., Jien, S.H., Mentler, A., Hein, T., Huang, J.C., Hseu,
539 Z.Y., Cheng, L.W., Yu, C.K., and Zehetner, F.: Soil aggregate breakdown and carbon release
540 along a chronosequence of recovering landslide scars in a subtropical watershed, *Catena*, in



- 541 revision, 2018.
- 542 Seibert, J., and Vis, M. J. P.: Teaching hydrological modeling with a user-friendly catchment-runoff-
543 model software package, *Hydrol. Earth Syst. Sci.*, 16, 3315-3325, [10.5194/hess-16-3315-2012](https://doi.org/10.5194/hess-16-3315-2012),
544 2012.
- 545 Stutter, M. I., Richards, S., and Dawson, J. J.: Biodegradability of natural dissolved organic matter
546 collected from a UK moorland stream, *Water Res.*, 47, 1169-1180,
547 [10.1016/j.watres.2012.11.035](https://doi.org/10.1016/j.watres.2012.11.035), 2013.
- 548 Tian, Y. Q., Yu, Q., Feig, A. D., Ye, C., and Blunden, A.: Effects of climate and land-surface
549 processes on terrestrial dissolved organic carbon export to major U.S. coastal rivers, *Ecol. Eng.*,
550 54, 192-201, [10.1016/j.ecoleng.2013.01.028](https://doi.org/10.1016/j.ecoleng.2013.01.028), 2013.
- 551 Walvoord, M. A., and Striegl, R. G.: Increased groundwater to stream discharge from permafrost
552 thawing in the Yukon River basin: Potential impacts on lateral export of carbon and nitrogen,
553 *Geophys Res Lett*, 34, 2007.
- 554 West, A. J.: Thickness of the chemical weathering zone and implications for erosional and climatic
555 drivers of weathering and for carbon-cycle feedbacks, *Geology*, 40, 811-814, 2012.
- 556 Winterdahl, M., Futter, M., Köhler, S., Laudon, H., Seibert, J., and Bishop, K.: Riparian soil
557 temperature modification of the relationship between flow and dissolved organic carbon
558 concentration in a boreal stream, *Water Resour. Res.*, 47, [10.1029/2010wr010235](https://doi.org/10.1029/2010wr010235), 2011.
- 559 Wymore, A. S., Brereton, R. L., Ibarra, D. E., Maher, K., and McDowell, W. H.: Critical zone
560 structure controls concentration-discharge relationships and solute generation in forested
561 tropical montane watersheds, *Water Resour. Res.*, 53, 6279-6295, [10.1002/2016wr020016](https://doi.org/10.1002/2016wr020016),
562 2017.
- 563 Yeh, T.C., Liao, C.S., Chen, T.C., Shih, Y.T., Huang, J.C., Zehetner, F., Hein, T.: Differences in N
564 loading affect DOM dynamics during typhoon events in a forested mountainous catchment.
565 *Science of the Total Environment* (submitted).
- 566 Zhong, J., Li, S. L., Tao, F. X., Yue, F. J., and Liu, C. Q.: Sensitivity of chemical weathering and
567 dissolved carbon dynamics to hydrological conditions in a typical karst river, *Scientific Reports*,
568 7, ARTN 42944 [10.1038/srep42944](https://doi.org/10.1038/srep42944), 2017.
- 569 Zhou, W.-J., Zhang, Y.-P., Schaefer, D. A., Sha, L.-Q., Deng, Y., Deng, X.-B., and Dai, K.-J.: The
570 role of stream water carbon dynamics and export in the carbon balance of a tropical seasonal
571 rainforest, southwest China, *PloS one*, 8, e56646, [10.1371/journal.pone.0056646](https://doi.org/10.1371/journal.pone.0056646), 2013.
- 572
- 573



574
 575

Table

576 **Table 1.** Performances of estimated DOC and DIC flux at the three sites using LOADEST.

	Site	Sample	Flux			Concentration	
		Number ^{*1}	R^2	Bp ^{*2}	NSE	R^2	NSE
DOC	T1	76	0.98	4.1	0.93	0.53	0.41
	T2	64	0.98	1.3	0.97	0.55	0.55
	M3	85	0.96	6.1	0.88	0.34	0.31
DIC	T1	65	0.98	0.4	0.94	0.60	0.58
	T2	42	0.97	3.2	0.95	0.63	0.50
	M3	67	0.97	3.1	0.98	0.51	0.59

577 ^{*1} Sample number varied among catchments due to differences in site accessibility associated
 578 with road damage caused by typhoons or equipment failure.

579 ^{*2} Bp indicates flux bias in percentage, defined as the estimated minus the observed values over
 580 the observed values

581

582 **Table 2.** Estimated concentrations and fluxes of DOC and DIC at the three sites during 2014-2015

Catchment	DOC	DIC	DOC	DIC
	conc. (μM)		flux ($\text{ton-C km}^{-2} \text{ period}^{-1}$)	
Annual				
T1	138	2099	3.5	53.4
T2	174	1951	4.8	54.3
M3	99	1805	2.7	48.4
Average	137	1951	3.7	52.1
Wet season				
T1	150	2097	3.3	46.7
T2	184	1890	4.7	48.6
M3	108	1798	2.5	42.6
Average	147	1928	3.5	45.9
Dry Season				
T1	53	2113	0.2	6.7
T2	55	2672	0.1	5.8
M3	37	1863	0.1	5.9
Average	48	2216	0.1	6.1

583

584



585

586 **Table 3.** The fluxes of DOC and DIC, their contributions to annual fluxes (%) and the relative
 587 contributions (%) from three sources (rapid surface runoff, subsurface runoff and deep groundwater)
 588 at site M3 during the two typhoon events.

		Q_{sim} mm/event	DOC kg-C km ² /event	DIC
Typhoon	Flux	248.4	382.5	3999.4
Matmo	Event/Annual	12%	15.0%	9.2%
	Rapid surface runoff	40%	40%	24%
	Subsurface runoff	24%	37%	19%
	Deep groundwater	37%	23%	57%
Typhoon	Flux	328.0	744.5	6790.3
Soudelor	Event/Annual	14%	23.5%	12.6%
	Rapid surface runoff	50%	48%	34%
	Subsurface runoff	25%	37%	22%
	Deep groundwater	25%	15%	44%

589

590



591 **Table 4.** The mean SMR annual concentrations and fluxes of DOC and DIC across the globe.

Region	Concentration (μM)		Flux ($\text{ton km}^{-2} \text{yr}^{-1}$)		DIC/DOC*	Ref.
	DOC	DIC	DOC	DIC		
Global	479	858	1.4	2.6	1.86	Meybeck and Vörösmarty, 1999
Small mountainous rivers^A	199	408	2.5	7.01	2.80	
Subarctic streams	222	279	1.52	2.03	1.34	Giesler et al., 2014
Temperate headwater	-	-	1.7	6.3	3.71	Argerich et al., 2016
Tropical seasonal rainforest	308	500	1.02	2.43	2.38	Zhou et al., 2013
Tropical volcanic islands ^L	75	513	2.5	19.6	6.60	Lloret et al., 2011
Tropical volcanic islands ^F	215	339	5.7	4.8	1.39	Lloret et al., 2011
Southwestern China(Karst)	88	2,472	1.5	41.0	27.30	Zhong et al., 2017
Oceania	399	1,781	8.0	34.0 ^G	4.25	Huang et al., 2012
Papua New Guinea	321	1,018	8.9	28.2	3.20	Alin et al., 2008
SE Australia Subtropical rivers	360	1,860	0.44	1.1 ^E	10.71-13.38	Atkins et al., 2017
Tseng-Wen River, Taiwan	137	1,951	3.7	52.1	14.08	This study

592 *DIC/DOC is calculated from either concentration or yield depending on data availability.

593 ^A the values were the average of the listed studies, but did not include Zhong et al. (2017), due to the
 594 specificity of karst landscape

595 ^L and ^F indicate low and high flow conditions, respectively.

596 ^E the discharge during the sampling period is only one-third of the long-term average due to the
 597 ENSO effect.

598 ^G the discharge (1572 mm yr^{-1}) that we used is consistent with the GRDC dataset, but ~10 times
 599 higher than the value reported by Huang et al., (2012).

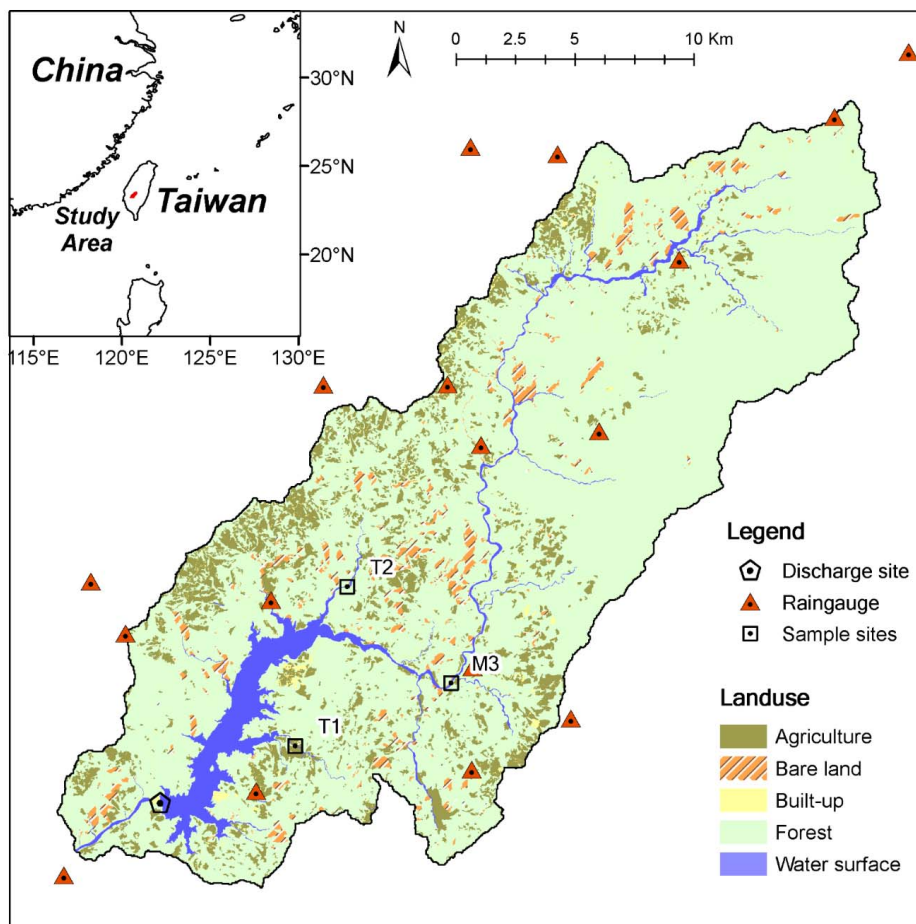
600



601

Figure

602

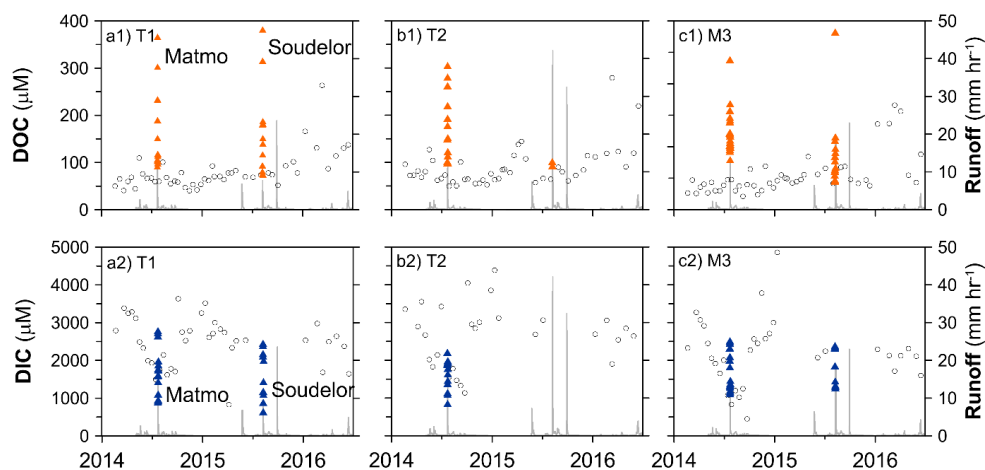


603

604 **Figure 1.** Location map of sampling sites, rain gauges and land cover pattern in Tsengwen

605 catchment.

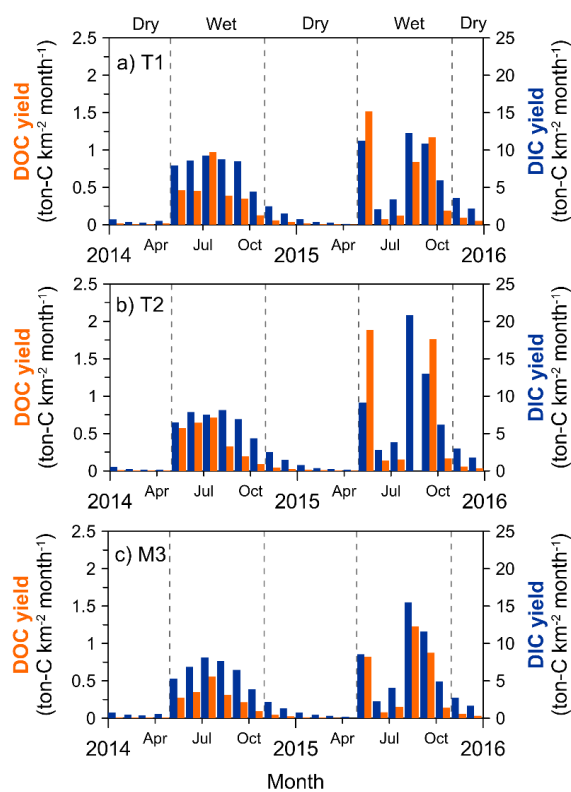
606



607

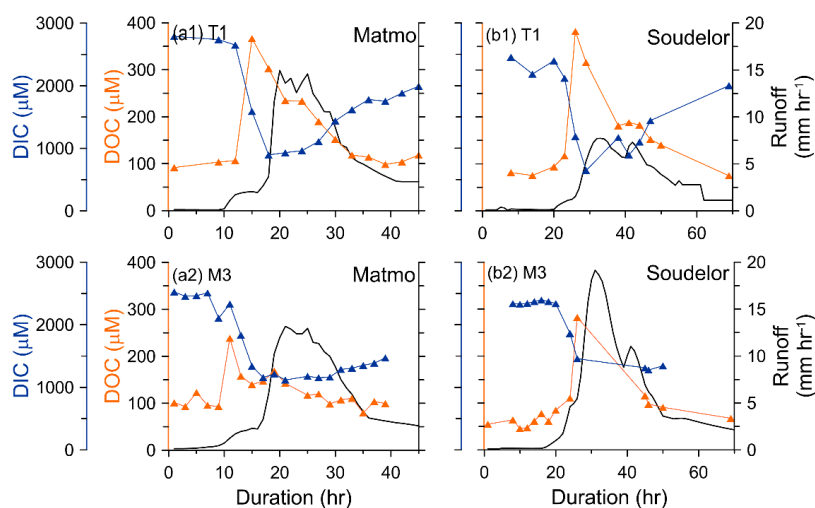
608 **Figure 2.** DOC (upper) and DIC (lower) concentration at the three sampling sites (left to right for
609 site T1, T2, and M3, respectively.) during 2014/01-2016/08. The gray line represents discharge and
610 the black circles represent results of biweekly sampling. The orange and blue solid triangles indicate
611 DOC and DIC of the high-frequency sampling during the two typhoon events.

612



613

614 **Figure 3.** The DOC and DIC yield (ton C km⁻² mon⁻¹) at the three sites. Sub-figure (a)~(c) indicate
615 the site T1, T2, and M3, respectively.



616

617 **Figure 4.** Temporal variation of DOC and DIC concentration during typhoon periods. The left panel

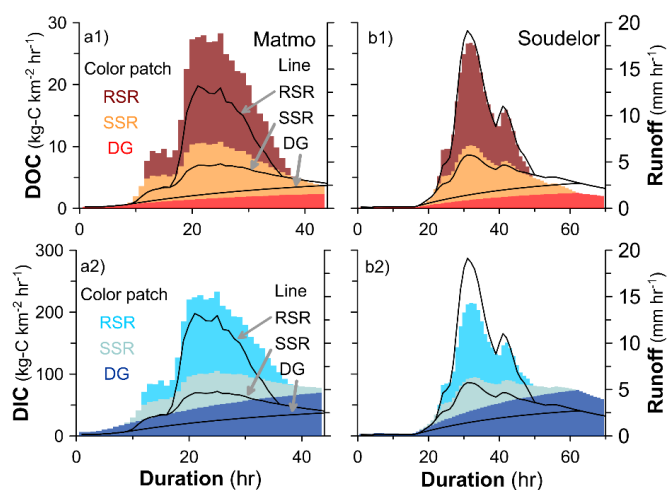
618 is Typhoon Matmo (2014-07-22~2014-07-24) and the right panel is Typhoon Soudelor (2015-08-

619 07~2015-08-10). Upper and lower plots are results of site T1 and M3, respectively.

620

621

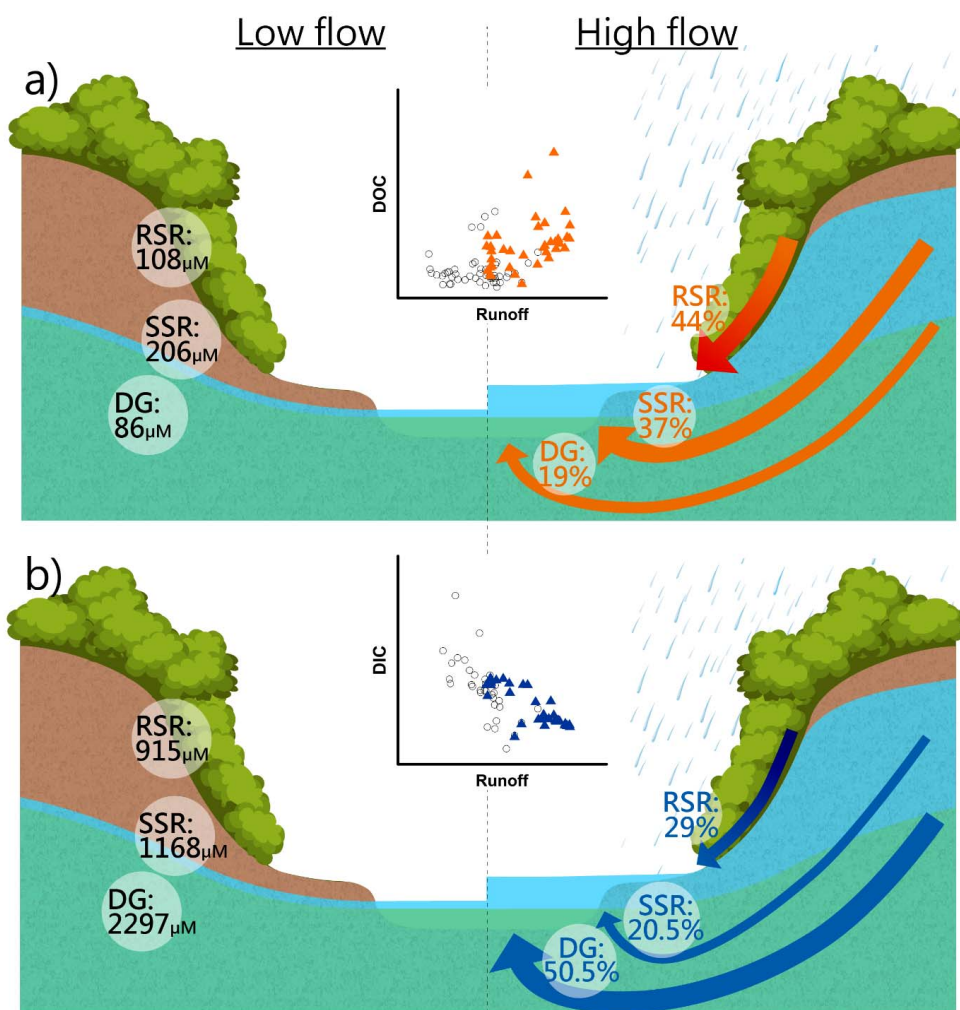
622



623

624 **Figure 5.** DOC and DIC from different sources during two typhoons at site M3. The stacked colored
625 patches present the flux of DOC and DIC from RSR (upper patch), SSR (middle patch) and DG
626 (lower patch). The region stack by black lines represents the hourly runoff from the three pathways
627 (RSR, SSR, and DG, from top to bottom, respectively).

628



629

630 **Figure 6.** Conceptual model for DOC (a) and DIC (b) transport from different sources at low and
 631 high flow regimes. The subplots in the center represent C-Q relation at low (black circle) and high
 632 flow regimes (solid triangle). Left half illustrates the DOC and DIC concentrations from different C
 633 sources and right half illustrates the proportional transport by different runoffs (e.g., RSR, SSR, DG).
 634 The values used for high flow was the average of the two typhoon events (Table 3).

635